



HAL
open science

Degradation of Acetaminophen via UVA-induced advanced oxidation processes (AOPs). Involvement of different radical species: HO \cdot , SO $_4^{\cdot-}$ and HO $_2$ /O $_2^{\cdot-}$

Xiaoning Wang, Marcello Brigante, Wenbo Dong, Zhangxiong Wu, Gilles Mailhot

► To cite this version:

Xiaoning Wang, Marcello Brigante, Wenbo Dong, Zhangxiong Wu, Gilles Mailhot. Degradation of Acetaminophen via UVA-induced advanced oxidation processes (AOPs). Involvement of different radical species: HO \cdot , SO $_4^{\cdot-}$ and HO $_2$ /O $_2^{\cdot-}$. *Chemosphere*, 2020, 258, pp.127268. 10.1016/j.chemosphere.2020.127268 . hal-02995763

HAL Id: hal-02995763

<https://hal.science/hal-02995763>

Submitted on 9 Nov 2020

HAL is a multi-disciplinary open access archive for the deposit and dissemination of scientific research documents, whether they are published or not. The documents may come from teaching and research institutions in France or abroad, or from public or private research centers.

L'archive ouverte pluridisciplinaire **HAL**, est destinée au dépôt et à la diffusion de documents scientifiques de niveau recherche, publiés ou non, émanant des établissements d'enseignement et de recherche français ou étrangers, des laboratoires publics ou privés.

1 **Degradation of Acetaminophen via UVA-induced advanced oxidation**
2 **processes (AOPs). Involvement of different radical species: HO[•],**
3 **SO₄^{•-} and HO₂[•]/O₂^{•-}**
4

5 Xiaoning Wang ^{a, b, c}, Marcello Brigante ^b, Wenbo Dong ^c, Zhangxiong Wu ^a, Gilles
6 Mailhot ^{*b},

7 **a:** Suzhou Key Laboratory of Green Chemical Engineering, School of Chemical and
8 Environmental Engineering, College of Chemistry, Chemical Engineering and
9 Materials Science, Soochow University, Suzhou, Jiangsu 215123, China

10 **b:** Université Clermont Auvergne, CNRS, SIGMA Clermont, Institut de Chimie de
11 Clermont-Ferrand, F-63000 Clermont-Ferrand, France

12 **c:** Shanghai Key Laboratory of Atmospheric Particle Pollution and Prevention,
13 Department of Environmental Science and Engineering, Fudan University, Shanghai
14 200433, China

15 * Corresponding Author:

16 E-mail: gilles.mailhot@uca.fr (Gilles Mailhot)

17

18

19

20

21

22

1 **Abstract**

2 In this work, UVA radiation that is part of solar light is taken as the irradiation
3 source and radicals (HO^\bullet , $\text{SO}_4^{\bullet-}$ and $\text{HO}_2^\bullet/\text{O}_2^{\bullet-}$) are generated through activation of
4 hydrogen peroxide (H_2O_2), sodium persulfate ($\text{Na}_2\text{S}_2\text{O}_8$) and Bismuth catalyst
5 (BiOCl), respectively. The distinguished performance in removing acetaminophen
6 (ACTP), a model pharmaceutical pollutant, by these three radicals was compared for
7 the first time. Effect of pH, halide ions concentration and interfacial mechanism have
8 been investigated in detail. Interestingly, results show that heterogeneous
9 UVA/ BiOCl process has higher degradation efficiency than homogeneous
10 UVA/ H_2O_2 and UVA/ $\text{Na}_2\text{S}_2\text{O}_8$ systems whatever the solution's pH. To explain these
11 results, second order reaction rate constant ($k_{\text{radical,ACTP}}$) have been determined with
12 laser flash photolysis (LFP) or radical scavenging experiments. The strongly
13 interfacial-dependent $\text{HO}_2^\bullet/\text{O}_2^{\bullet-}$ radicals have the lowest second order rate constant
14 with ACTP but highest steady state concentration. BiOCl was much easier activated
15 by UVA, and outstanding ACTP mineralization can be achieved. Combination of
16 BiOCl and $\text{Na}_2\text{S}_2\text{O}_8$ exhibits synergistic effects rather than antagonism effects with
17 H_2O_2 . This study highlights the relative effective utilization of solar light through
18 interfacial directed BiOCl photocatalysis and its synergistic effects with traditional
19 oxidants.

20

21 **Key words:** advanced oxidation process, photocatalysis, UVA, radicals, synergistic
22 effects

1 **1 Introduction**

2 In recent years, advanced oxidation processes (AOPs) have been proposed as
3 alternative methods to effectively remove persistent organic pollutants (POPs) in
4 environment. Normally, AOPs have always proved to achieve the best yields in
5 pollutant destruction when biological treatments are unfeasible, like for endocrine
6 disrupting chemicals (EDCs) (Pera-Titus et al., 2004; Rosenfeldt and Linden, 2004),
7 pharmaceuticals or personal care products (PPCPs) (Huber et al., 2003; Abdelmelek et
8 al., 2011). The predominant oxidation processes are usually based on H₂O₂ or
9 persulfate activation by *in situ* production of hydroxyl radical (HO[•]) or sulfate radical
10 (SO₄^{•-}), followed by reaction on the targets pollutants in aqueous solutions
11 (Andreozzi et al., 1999; Esplugas et al., 2002). Especially, traditional Fenton reaction
12 (Fe(II)/H₂O₂) (Neyens and Baeyens, 2003; Huang et al., 2013) and UV/H₂O₂ are
13 predominant strategies to generate HO[•]. Similarly, SO₄^{•-} are always produced through
14 activation of persulfate by heat (Nie et al., 2014), UV, alkalinity (Nie et al., 2019) and
15 transition metals (Wu et al., 2015a). However, Fenton reactions always suffer from
16 several limitations like strict acidic solution (pH < 4.0) and iron sludge disposal.

17 At the same time, interfacial based heterogeneous photocatalysis is also one of
18 the most promising oxidation processes through producing electron (e⁻) and hole (h⁺)
19 pairs under illumination. HO[•] or hydroperoxyl radicals/superoxide radical anion
20 (HO₂[•]/O₂^{•-}, pKa 4.88) will be subsequently produced by reaction of photogenerated
21 charge carriers with O₂ and H₂O (Shaban et al., 2013). Among these photocatalysts,
22 TiO₂ and its doped products have received a great deal of attention due to its efficient

1 and abundant production of HO[•] (Yang et al., 2008a). Different to TiO₂, in
2 bismuth-related photocatalytic process, especially layered BiOX (X = Cl, Br, I)
3 (Zhang et al., 2008), quenching experiments and theoretical calculation have proved
4 that they are featured with HO₂[•]/O₂^{•-} generation for organic compound degradation
5 (Tian et al., 2019). Taking BiOCl as catalyst, the photocatalytic process can supply a
6 simple route to produce HO₂[•]/O₂^{•-} effectively. In our last studies, a series of BiOCl
7 related catalysts have been synthesized by precipitation method successfully followed
8 with detailed characterization (Wang et al., 2014, 2016a, 2016b). BiOCl possesses
9 great surface area and suitable valance/conduction band structures to produce
10 HO₂[•]/O₂^{•-} active species, showing excellent performance in removing acetaminophen
11 (ACTP) from water under irradiation ($\lambda > 290$ nm), although the band gap value of
12 BiOCl (~ 3.2 eV) shows that it only can be activated by the ultraviolet light with the
13 wavelength shorter than 387.5 nm. Similar to the previous literatures, HO₂[•]/O₂^{•-}
14 species are the main radical determined by indirect scavenging experiments.

15 If UVA radiation (315–400 nm) is chosen as the irradiation source, H₂O₂ and
16 persulfate as the oxidation sources, the quantum yield comparison between HO[•] and
17 SO₄^{•-} still stay unknown. Furthermore, nobody has compared these two radicals with
18 HO₂[•]/O₂^{•-} under the same experimental conditions. The degradation rate of organic
19 pollutant depends on the radical concentration, selectivity and oxidizing power. For
20 these reasons, the distinguished and cumulated effects of these parameters need to be
21 explored. ACTP was chosen as the model pollutant in this study, because of its heavy
22 use all over the world. Most of the research on ACTP degradation are mainly based on

1 HO[•] and SO₄^{•-} like UV/H₂O₂ (Andreozzi et al., 2003), Fenton (de Luna et al., 2013),
2 TiO₂ photocatalyst (Yang et al., 2008b) and persulfate activation (Noorisepehr et al.,
3 2019; Yun et al., 2019). Its degradation pathway by HO[•] and SO₄^{•-} are almost clear,
4 while its degradation and mineralization abilities by HO₂[•]/O₂^{•-} still stays largely
5 unknown. Furthermore, the combination of TiO₂ with H₂O₂ (Li et al., 2001) or
6 persulfate activation (Xu et al., 2019) has been widely investigated. However, rare
7 studies focus on the synergistic effects between BiOCl with H₂O or persulfate (Zhang
8 et al., 2017).

9 In brief, the main goal of this paper is to compare, for the first time, three
10 different active species HO[•], SO₄^{•-} and HO₂[•]/O₂^{•-} produced by UVA/H₂O₂,
11 UVA/Na₂S₂O₈ and UVA/BiOCl respectively on the degradation of ACTP. pH and
12 halide ions (Cl⁻ and I⁻) concentration effects on ACTP's degradation have been
13 investigated in this work. The combination of oxidants in the systems
14 UVA/BiOCl/H₂O₂ and UVA/BiOCl/Na₂S₂O₈ are also studied to explore the potential
15 synergistic effects. Interfacial mechanism, mineralization and efficiency of this
16 process will be explained in detail. Furthermore, second order reaction rate constants
17 between ACTP and HO[•], SO₄^{•-} or HO₂[•]/O₂^{•-} radicals will be determined by laser flash
18 photolysis (LFP) or competition experiments. The critical affecting parameters on
19 ACTP's degradation rate will be determined.

20 **2 Materials and methods**

21 **2.1 Chemicals**

22 BiOCl catalyst was synthesized as in our previous papers (Wang et al., 2016a).

1 ACTP was purchased from Sinopharm Chemical Reagent Co., Ltd. (China).
2 Bisphenol A (BPA), $\text{NaH}_2\text{PO}_4 \cdot \text{H}_2\text{O}$, NH_4SCN , ethanol (EtOH), tert-butanol (TBA),
3 sodium persulfate ($\text{Na}_2\text{S}_2\text{O}_8$), benzoquinone (BQ) and potassium iodine (KI) were
4 obtained from Sigma, France. Hydrogen peroxide (H_2O_2) solution (30% in water) and
5 sodium chloride (NaCl) were purchased from Fluka, France.
6 5,5-Dimethyl-1-pyrroline N-Oxide (DMPO, 98%) was obtained from Adamas
7 Reagent Co., Ltd. Perchloric acid (HClO_4) and sodium hydroxide (NaOH) were used
8 to adjust the pH of the solutions. All chemicals were used without further purification,
9 and milli-Q water was used throughout all the experiments.

10 ***2.2 Irradiation setup and experimental procedure***

11 The photocatalytic degradation experiments were performed in a homemade
12 photoreactor placed in a cylindrical stainless steel container. Four fluorescent
13 lightbulb lamps (Philips TL D15W/05) were separately placed in the four different
14 axes while the photoreactor, a water-jacketed Pyrex tube of 2.8 cm internal diameter,
15 was placed in the center of the setup. The lamp emitting from 300 to 500 nm was used
16 to simulate UVA solar light; their emission spectrum is shown in **Fig. S1**. 100 mL of
17 solutions were magnetically stirred with a magnetic bar during irradiation and
18 experiments were carried out at room temperature (293 ± 2 K) set by a circulating
19 cooling water system. Samples were taken from the reaction tube at fixed interval
20 times and the catalyst solid was removed by $0.22 \mu\text{m}$ PTFE filters before analysis. In
21 the experiments, the initial concentrations used were: ACTP $50 \mu\text{M}$, H_2O_2 and
22 $\text{Na}_2\text{S}_2\text{O}_8$ 1 mM and BiOCl catalyst 0.3 g L^{-1} (approximately 1.1 mM). All experiments

1 were performed in duplicates, experimental points represent the averages of two
2 values, and the error bars indicate the standard deviation.

3 ***2.3 Analytical method***

4 The remaining ACTP concentration in the aqueous solution was determined by
5 high performance liquid chromatography (HPLC) (Alliance, Waters, 2695, USA)
6 equipped with a photodiode array detector (Waters 2998). A Nucleodur 100-3 C18
7 reverse column (150 × 2.0 mm, 3.0 μm) was used to separate the compound in the
8 solution. The flow rate was 0.15 mL min⁻¹ with a mobile phase mixture of methanol
9 and water with 0.1% H₃PO₄ (30/70, v/v). The UV detection of ACTP was set at 244
10 nm wavelength, and the retention time was 4.9 min. Mineralization of ACTP solution
11 was followed by total organic carbon (TOC) analysis (5050A, Shimadzu, Japan).
12 UV–vis spectra were recorded with a Cary 300 UV–visible spectrophotometer. pH
13 values of the solutions were measured using a Cyberscan 510 pH meter. The zeta
14 potential of BiOCl was determined by the potentiometric titration method under N₂
15 atmosphere at 298 K in 1 mM NaCl solutions. X-ray photoelectron spectroscopy
16 (XPS) spectra were collected by using a VG Scientific ESCALAB 250Xi
17 spectrometer (Thermo Fisher Scientific) with C 1s as the calibration standard line.
18 The optical properties of BiOCl samples were analyzed through the UV–vis diffuse
19 reflectance (DRS) by Shimadzu UV-3600. The electron spin resonance (ESR)
20 experiments were carried out on a JES-X320 spectrometer to detect the reactive
21 radicals generated over the photocatalytic degradation process. As radical probe,
22 DMPO (100 mM) was used for SO₄^{•-}, HO[•] and HO₂[•]/O₂^{•-}. ESR spectrum was

1 recorded at room temperature under the following operating conditions: a modulation
2 frequency of 100 kHz, a sweep width of 0.5 mT, a microwave power of 1 mW, a
3 microwave frequency of 9.15 GHz and a centerfield of 326.0 ± 5 mT.

4 ***2.4 Determination of the second order rate constant***

5 For the detection of second order rate constant between ACTP and HO \cdot ($k_{\text{ACTP, HO}\cdot}$,
6 HO \cdot), LFP method was adopted. Experiments were carried out using the fourth
7 harmonic ($\lambda_{\text{exc}} = 266$ nm) of a Quanta Ray GCR 130-01 Nd: YAG laser system
8 instrument and the energy was set as approximately 45 mJ/pulse. Other conditions
9 were kept the same to those described in previous articles ([Brigante et al., 2010](#);
10 [Huang et al., 2018](#)). High concentrated stock solutions (ACTP, H $_2$ O $_2$ and SCN $^-$) were
11 mixed just before each experiment and diluted with Mili-Q water to obtain the desired
12 mixtures and concentrations in a 3 mL quartz cuvette. The value of $k_{\text{ACTP, HO}\cdot}$ can be
13 obtained through mixing SCN $^-$ (0.1 mM), H $_2$ O $_2$ (5.5 mM) with different
14 concentrations of ACTP in the quartz cell. The detection wavelength was set at 475
15 nm to detect maximum absorbance of SCN $_2^{\bullet-}$. The specific detection calculation was
16 shown in [Scheme S1](#) and [Equations S1-S4](#).

17 For the detection of second order rate constant of sulfate radical on ACTP ($k_{\text{ACTP, SO}_4^{\bullet-}}$,
18 SO $_4^{\bullet-}$), competition method was adopted by taking BPA as the competitor ([Ji et al.,](#)
19 [2013](#)), because $k_{\text{SO}_4^{\bullet-}, \text{BPA}} = 4.7 \times 10^9 \text{ M}^{-1} \text{ s}^{-1}$ has been detected in previous studies by
20 LFP ([Huang et al., 2018](#)). For this experiment, BPA (50 μM) and ACTP (50 μM)
21 were undergoing competition reactions under Na $_2$ S $_2$ O $_8$ (1 mM)/UVA at pH 5.4 for 240
22 min. At this pH conditions, sulfate radical prevailed with negligible hydroxyl radical

1 existence (Fang et al., 2013a). The concentrations of BPA and ACTP were followed at
 2 different treatment time intervals and the rate constant of ACTP with $\text{SO}_4^{\bullet-}$ can be
 3 calculated through **Eq.1**.

$$4 \quad k_{\text{ACTP},\text{SO}_4^{\bullet-}} = k_{\text{BPA},\text{SO}_4^{\bullet-}} \times \frac{\ln\left(\frac{[\text{ACTP}]_t}{[\text{ACTP}]_0}\right)}{\ln\left(\frac{[\text{BPA}]_t}{[\text{BPA}]_0}\right)} \quad (1)$$

5

6 **3 Results and Discussion**

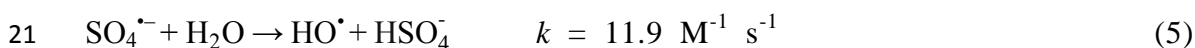
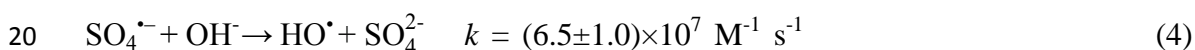
7 **3.1 ACTP degradation in UVA/H₂O₂ and UVA/Na₂S₂O₈ systems under different pH**

8 To explore ACTP's degradation with H₂O₂ and Na₂S₂O₈ under UVA irradiation,
 9 blank experiments were firstly conducted in the dark to check its stability. ACTP
 10 alone in aqueous solution is stable between pH 3-9.5 within 40 hours (Fig.S2A). In
 11 addition, when ACTP was mixed with H₂O₂ and Na₂S₂O₈ (Fig.S2B, C), no detectable
 12 degradation can be observed until pH 9.0, while at higher pH a degradation was
 13 measured particularly with persulfate.

14 Degradation of ACTP with H₂O₂ and Na₂S₂O₈ under UVA during irradiation are
 15 shown in Fig.1, and all the reactions follow pseudo first order reaction kinetics (data
 16 are shown in Fig.4C). From the control experiment, direct photolysis of ACTP could
 17 be neglected (Fig.1A). Results of quenching experiments demonstrated that HO[•] and
 18 $\text{SO}_4^{\bullet-}$ are the predominant radicals involved in the UVA/H₂O₂ and UVA/Na₂S₂O₈
 19 system (Eq.2-3) at pH 5.4 respectively by taking IPA (10 mM) and EtOH (1 M) as
 20 HO[•] ($k_{\text{IPA}, \text{HO}^{\bullet}} = 1.9 \times 10^9 \text{ M}^{-1} \text{ s}^{-1}$) (Wu et al., 2017) and $\text{SO}_4^{\bullet-}$ ($k_{\text{EtOH}, \text{SO}_4^{\bullet-}} = 1.6-7.7 \times 10^7$
 21 $\text{M}^{-1} \text{ s}^{-1}$) (Tan et al., 2014) scavengers, respectively. No direct photolysis of ACTP was

1 observed under UVA radiation. With H₂O₂ or Na₂S₂O₈ addition to the solution, ACTP
 2 shows different degradation kinetics under various pH. In general, UVA/Na₂S₂O₈
 3 shows a higher degradation efficiency than UVA/H₂O₂ system whatever the solution's
 4 pH. It has been reported that H₂O₂ only can be activated by the light at $\lambda < 320$ nm,
 5 which almost have been confirmed in this research for the weak degradation in
 6 UVA/H₂O₂ (Li et al., 2001). The obvious degradation of ACTP in UVA/Na₂S₂O₈
 7 indicates that Na₂S₂O₈ is easier to be activated than H₂O₂ under UVA irradiation.

8 In UVA/H₂O₂ system, slightly acidic solution has the maximum removal
 9 percentage rather than acidic and alkaline solutions, although the maximum removal
 10 is only approximately 10%. In contrast, degradation rate is increasing with pH further
 11 increasing (Fig.1B) in UVA/Na₂S₂O₈ system, and about 57% ACTP can be removed at
 12 pH 10. At least two reasons are involved simultaneously to account for this
 13 phenomenon. Firstly, Fig.S2B has been taken into consideration, ACTP is easier to be
 14 oxidized in anionic form. Furthermore, alkaline solution favors more formation of
 15 HO[•] radicals from SO₄^{•-} than neutral pH (Eq.4-5) (Fang et al., 2013a), and these two
 16 radicals have different second order reaction rate constants with ACTP, which will be
 17 explained in the following part.



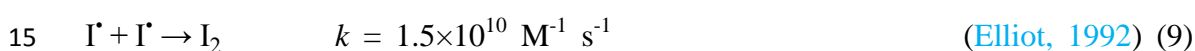
22 **3.2 Halide ions (chloride and iodide) effects on ACTP degradation in UVA/H₂O₂**

1 *and UVA/Na₂S₂O₈ systems*

2 Effects of halide ions were widely studied in previous research works, especially
3 chloride and bromide (Tamtam and Chiron, 2012; Li et al., 2015). In our study for the
4 first time the comparison of Cl⁻ and I⁻, which is also commonly detected in costal
5 seawater, saline water or industrial wastewater discharges, were investigated in
6 UVA/H₂O₂ and UVA/Na₂S₂O₈ systems. In the dark and whatever the systems, the
7 addition of Cl⁻ has no impact on ACTP's concentration change (see Fig.S3). Under
8 irradiation, the impact of Cl⁻ is also very weak. The only effect is observed in the
9 UVA/H₂O₂ system, when NaCl is set as 10 mM, the pseudo first order reaction rate
10 constant increase around 30% (see Fig.S4). In the presence of chloride ions, generated
11 reactive species such as chlorine radical (Cl[•]) and dichlorine radical anion (Cl₂^{•-})
12 could react more selectively with electron-rich organic compounds (Grebel et al.,
13 2010).

14 On the contrary, when iodide ions at same concentrations were added to the
15 solution, ACTP degradation rates are strongly affected as shown in Fig.2. In the dark,
16 the addition of KI from 260 μM to 5 mM leads to an increase of the ACTP
17 degradation with H₂O₂, which is much less the case with Na₂S₂O₈ at pH 5.4. In the
18 presence of H₂O₂ or Na₂S₂O₈, iodide ions could be oxidized to iodine I₂ (Eq.6). Under
19 UVA irradiation, KI alone in solution has no effect on ACTP (Fig.S5), indicating that
20 iodide ions under UVA cannot transform or generate any active species. However, in
21 the presence of H₂O₂ or Na₂S₂O₈ in the KI solution, the photo-degradation rate is
22 highly enhanced (Fig. 2). In addition, HOI^{•-}/I^{•-} reactive halogenated species can be

1 generated from HO[•] or SO₄^{•-} as shown in **Eq.7-8** (Elliot, 1992), indicating that iodide
 2 radicals (I[•], HOI^{•-} and I₂^{•-}) have higher reactivity with organic pollutants than chloride
 3 radicals (Yang et al., 2018a). Tamtam and Chiron (2012) and Li et al. (2015) have
 4 demonstrated that reactive halogenated species reacted more selectively than hydroxyl
 5 radicals with electron-rich organic pollutants. As ACTP contains hydroxyl and
 6 acetamido groups, which are electron donors to the aromatic rings, so it is
 7 hypothesized that these electron-rich moieties may selectively react with these iodide
 8 related radical reactive species. These selectivity properties of iodide based radicals
 9 are more emphasized than chloride ions. However, too much higher concentrated
 10 iodide ions (5 mM) will decrease the efficiency of ACTP degradation by
 11 self-quenching effects (**Eq.9**).



16 **3.3 ACTP's degradation performance in BiOCl/UVA system**

17 Heterogeneous photocatalytic degradation of ACTP has attracted numerous
 18 attentions recently, and various degradation pathways have been proposed for SO₄^{•-}
 19 and HO[•] reactivity on ACTP. On the contrary, seldom studies have investigated the
 20 degradation of ACTP predominantly by superoxide radicals. In our previous studies
 21 (Wang et al., 2016a), BiOCl catalyst has been synthesized following with detailed
 22 characterization properties, as shown in **Table 1**. The XPS characterization is

1 presented in Fig.S6, the valance state of each element is in accordance with previous
2 literatures, suggesting that BiOCl is well crystal organized with high purity. With a
3 relatively wide band-gap (3.2 eV), BiOCl could hardly absorb the light wavelengths
4 longer than 400 nm (Fig. S7A, B). The valance band of BiOCl determined from XPS
5 spectra is 2.2 eV (Fig. S7C), which is not positive enough to oxidize H₂O to form
6 hydroxyl radicals ($E^0(\text{H}_2\text{O}/\text{HO}^\bullet) = 2.8 \text{ V vs NHE}$) (Wu et al., 2015b). Accordingly, the
7 conduction band position can be calculated to be -1 eV, that is sufficiently negative
8 enough to combine with dissolve oxygen to generate $\text{HO}_2^\bullet/\text{O}_2^{\bullet-}$ ($E^0(\text{O}_2/\text{O}_2^{\bullet-}) = -0.28 \text{ V}$
9 vs NHE) (Wu et al., 2015b). Consequently, UVA/BiOCl is adopted to produce
10 $\text{HO}_2^\bullet/\text{O}_2^{\bullet-}$ radicals, which is further confirmed by quenching experiments (Fig.3A). In
11 fact, no inhibition is obtained in the presence of TBA (1 mM) and KI (1 mM), which
12 are traps of hydroxyl radicals and holes. Strong inhibition is noted with BQ (2 mM)
13 which is able to trap also superoxide radicals. Furthermore, the obvious inhibition in
14 N₂ purging condition further verifies that $\text{HO}_2^\bullet/\text{O}_2^{\bullet-}$ originate from the reaction
15 between dissolved oxygen and electrons.

16 Before irradiation, adsorption capacity of the catalyst is tested and the results
17 show that less than 10% of ACTP are adsorbed whatever the pH. Under irradiation,
18 pH effects are investigated and strong increase of the ACTP degradation is observed
19 at pH 3.0 if we compare with pH 5.8 and 7.5 (Fig.3B). These results are consistent
20 with previous reports about BiOX used as photocatalyst (Gao et al., 2015; Liang et al.,
21 2015) and the speciation of $\text{HO}_2^\bullet/\text{O}_2^{\bullet-}$ (pKa of 4.88) can explain the effect of pH (Li et
22 al., 2017). Indeed, the second order rate constant between $\text{O}_2^{\bullet-}$ with phenol is 5.8×10^2

1 $M^{-1} s^{-1}$ (Tsujiimoto et al., 1993) and Kozmér et al. have demonstrated that in acidic
2 solutions, HO_2^{\bullet} shows a higher reactivity with phenol $2.7 \times 10^3 M^{-1} s^{-1}$ (Kozmér et al.,
3 2014), which is reasonably similar for phenolic compound ACTP. Furthermore,
4 Zeta-potential of BiOCl is more negative with pH increasing (see Fig.3C), so less
5 photo-induced electrons can transferred to the surface to combine with oxygen
6 because electrostatic repulsion. While, as discussed above, electrons are crucial to
7 form $HO_2^{\bullet}/O_2^{\bullet-}$. In terms of organic compounds mineralization, UVA/BiOCl shows
8 excellent degradation and mineralization abilities compare to H_2O_2 or $Na_2S_2O_8$
9 whatever the solution's pH (Fig.3D).

10 ***3.4 Heterogeneous interfacial mechanism in UVA/BiOCl***

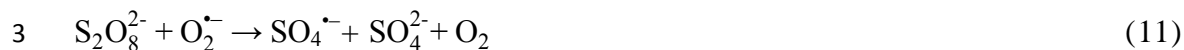
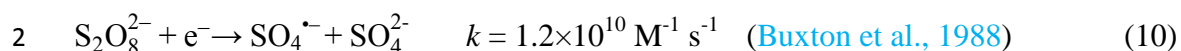
11 For heterogeneous photocatalytic degradation, interfacial mechanism is essential
12 to be investigated to confirm if the reaction is occurring in the solution or on the
13 surface of catalyst. To clarify this question, NaH_2PO_4 has been proved to be a perfect
14 desorbent in our experiment. Because NaH_2PO_4 could occupy almost all the
15 adsorption sites on the surface of catalyst, and the surface was tightly surrounded by
16 NaH_2PO_4 molecules instead of ACTP (Wang et al., 2018). With the addition of
17 NaH_2PO_4 , the degradation rate and removal percentage are both strongly suppressed
18 (Fig.4A). As we discussed above, the main active species $HO_2^{\bullet}/O_2^{\bullet-}$ comes from the
19 combination of dissolved oxygen in water and conduction band electrons. With a very
20 short half-life time, $HO_2^{\bullet}/O_2^{\bullet-}$ would easily undergo disproportionation (Liang et al.,
21 2015). Consequently, the fast and direct contact of pollutant and catalyst surface is
22 crucial for the reaction. Furthermore, BiOCl nanosheets prepared in alkaline

1 conditions in this research were usually dominated with high [010] facets exposure.
2 The [010] facets possessed open channels and abundant unsaturated Lewis/base sites,
3 which was helpful for intimate contact between the interfacial surface and organic
4 molecules (Jiang et al., 2012). So in this photocatalytic degradation system,
5 degradation reactions must be occurred on the surface or very close to the surface of
6 the catalyst.

7 ***3.5 Combination effects between H₂O₂, Na₂S₂O₈ and BiOCl under UVA***

8 Degradation of ACTP is investigated in H₂O₂/BiOCl/UVA and
9 Na₂S₂O₈/BiOCl/UVA systems to explore the possible synergy effects between H₂O₂ or
10 Na₂S₂O₈ and BiOCl, as shown in Fig.4B, C. It is obvious that UVA/BiOCl/Na₂S₂O₈ (k =
11 $7.13 \times 10^{-4} \text{ s}^{-1}$) exhibit strong synergy effects compared with UVA/Na₂S₂O₈ (k =
12 $4.63 \times 10^{-5} \text{ s}^{-1}$) and UVA/BiOCl ($k = 1.42 \times 10^{-4} \text{ s}^{-1}$) through accelerating ACTP's
13 removal and mineralization rate (Fig.4B, 3D). The increased degradation can be
14 ascribed to the following reasons. Firstly, the direct photolysis of S₂O₈²⁻ generating
15 SO₄^{•-} could contribute to the oxidation of ACTP. Secondly, S₂O₈²⁻ also can trap the
16 photogenerated conduction band electrons result in the formation of SO₄^{•-} (Eq.10)
17 (Sarwan et al., 2012). For the third reason, previous research has demonstrated the
18 reaction of O₂^{•-} with persulfate anion to generate SO₄^{•-} according to Eq.11 (Fang et
19 al., 2013b). However, addition of H₂O₂ slows down the degradation rate associated
20 with TOC removal (Fig.4B, C and 3D). The higher O–O bond energy of H₂O₂
21 compared with the band in free persulfate ions under natural pH could explain why
22 persulfate is easier to be activated than H₂O₂ by the same ROS (reactive oxygen

1 species) (Zhang et al., 2017).



4 ESR spectrum was performed to confirm the active species formed in this system
5 (Fig.5). No signal was detected in UVA/BiOCl system even repeat for several times or
6 with higher catalyst loading. This result is consistent with the results in paragraph 3.4,
7 which indicates that $\text{HO}_2^{\bullet}/\text{O}_2^{\bullet-}$ species may mainly exist on the surface of catalyst,
8 leaving trace amount dissolved in aqueous solutions, which is too low to be detected.
9 With the addition of H_2O_2 to the photocatalytic process, very weak HO^{\bullet} signals can be
10 observed due to its trace concentrations. While, with the addition of $\text{Na}_2\text{S}_2\text{O}_8$, stronger
11 HO^{\bullet} signal associating with $\text{HO}_2^{\bullet}/\text{O}_2^{\bullet-}$ signal can be observed. It is well known that
12 $\text{SO}_4^{\bullet-}$ -DMPO is very hard to be detected because of its rapid transformation to
13 HO^{\bullet} -DMPO (Yang et al., 2018b). $\text{SO}_4^{\bullet-}$ is indeed the main active species in natural
14 and acidic solutions. Above all, the addition of $\text{Na}_2\text{S}_2\text{O}_8$ facilitates the formation of
15 $\text{SO}_4^{\bullet-}$ and make full use of $\text{HO}_2^{\bullet}/\text{O}_2^{\bullet-}$ by driving them from surface to aqueous
16 solutions, which all contribute to higher mineralization abilities as shown in Fig.3D.

17 ***3.6 Determination of second order reaction rate constant between ACTP and HO^{\bullet} ,*** 18 ***$\text{SO}_4^{\bullet-}$ and $\text{HO}_2^{\bullet}/\text{O}_2^{\bullet-}$ radicals***

19 From the results discussed above, conclusions can be drawn that under same
20 illuminations, the degradation rate of ACTP follows: $\text{UVA/BiOCl} > \text{UVA/Na}_2\text{S}_2\text{O}_8 >$
21 $\text{UVA/H}_2\text{O}_2$, which mainly depends on the second order reaction rate constant (k_{ACTP} ,
22 radical) and radical's concentrations. $k_{\text{ACTP,HO}^{\bullet}}$ was determined from Eq.S1-S4 and

1 **Scheme S1**, by following the absorbance of $\text{SCN}_2^{\bullet-}$ at 475 nm using different ACTP
2 concentrations. The absorbance decreased from 0.021 to 0.006 when concentration of
3 ACTP increases from 0 to 2.33×10^{-4} M (**Fig.S8A**), because ACTP compete with
4 SCN^- to react with HO^\bullet . The slope “a” can be obtained from the linear regression of
5 Abs_0/Abs versus different ACTP concentrations, and it was equal to 11276. Thus the
6 second order constant $k_{\text{ACTP},\text{HO}^\bullet}$ can be evaluated from the product of “a”,
7 concentration of SCN^- (1×10^{-4} M) and $k_{\text{HO}^\bullet,\text{SCN}^-} = 1.2 \times 10^{10} \text{ M}^{-1} \text{ s}^{-1}$ (**Motohashi and**
8 **Saito, 1993**), finally it was calculated to be $1.35 \times 10^{10} \text{ M}^{-1} \text{ s}^{-1}$.

9 From competition method (**Fig.S8B**), $k_{\text{SO}_4^{\bullet-},\text{ACTP}} = 6.44 \times 10^9 \text{ M}^{-1} \text{ s}^{-1}$ was
10 determined. For $k_{\text{HO}_2^\bullet/\text{O}_2^{\bullet-},\text{ACTP}}$, reference’s results, already mentioned in part 3.3
11 ($5.8 \times 10^2 \text{ M}^{-1} \text{ s}^{-1}$ for $\text{O}_2^{\bullet-}$ and $2.7 \times 10^3 \text{ M}^{-1} \text{ s}^{-1}$ for HO_2^\bullet) are took into account and
12 because it has similar oxidation abilities towards phenolic compounds.

13 The steady state concentration of each radical ($[\text{Radical}]_{\text{SS}}$) can be estimated
14 from the pseudo first degradation constant of ACTP in three systems determined in
15 **Fig.S8C**. Considering that the pseudo first-order kinetic constant (k' , s^{-1}) is equal to
16 $k_{\text{radical},\text{ACTP}} \times [\text{Radical}]_{\text{SS}}$, we can estimate the steady state concentration of each
17 radical as $[\text{Radical}]_{\text{SS}} = k_{\text{radical},\text{ACTP}} / k'$, where $k_{\text{radical},\text{ACTP}}$ is the second order rate
18 constant between ACTP and selected radical. Under adopted experimental conditions,
19 a steady state concentration of HO^\bullet and $\text{SO}_4^{\bullet-}$ was determined to be 1.0×10^{-15} and
20 7.2×10^{-15} M respectively while for $\text{HO}_2^\bullet/\text{O}_2^{\bullet-}$ was in the range 10^{-8} - 10^{-7} M (**Table 2**).
21 Although $\text{HO}_2^\bullet/\text{O}_2^{\bullet-}$ radical has the weakest oxidation capacities, its concentration is
22 7-8 orders of magnitude higher than HO^\bullet and $\text{SO}_4^{\bullet-}$ radicals, thus directing the fast

1 degradation and mineralization efficiency of ACTP. From the view of economic, H_2O_2
2 and $\text{Na}_2\text{S}_2\text{O}_8$ are cheaper than the as-prepared BiOCl . But, it's essential to note that,
3 H_2O_2 and $\text{Na}_2\text{S}_2\text{O}_8$ are gradually consumed in solution under irradiation and as a
4 contrary, BiOCl catalyst, which is stable and can be preserved after catalytic reaction,
5 has the advantage of easy recovery and so to be recyclable.

6 **Conclusion**

7 In summary, heterogeneous photocatalytic process UVA/ BiOCl was always more
8 efficient than the homogeneous UVA/ H_2O_2 and UVA/ $\text{Na}_2\text{S}_2\text{O}_8$ processes to degrade
9 ACTP whatever the solution's pH. Halide ions such Cl^- plays a negligible role in
10 UVA/ H_2O_2 and UVA/ $\text{Na}_2\text{S}_2\text{O}_8$ systems, while I^- could significantly improve the
11 degradation performance due to the reactive species formation. BiOCl catalyst can be
12 efficiently activated by solar light than traditional oxidant such as H_2O_2 and $\text{Na}_2\text{S}_2\text{O}_8$.
13 With the same amount of oxidant or catalyst loading, UVA/ BiOCl system could
14 produce higher concentration of $\text{HO}_2^\bullet/\text{O}_2^{\bullet-}$ radicals, compared to HO^\bullet and $\text{SO}_4^{\bullet-}$. This
15 surface-depended $\text{HO}_2^\bullet/\text{O}_2^{\bullet-}$ oxidation process could induce significant mineralization
16 abilities. Addition of $\text{Na}_2\text{S}_2\text{O}_8$ shows synergistic effects in UVA/ BiOCl compared to
17 the addition of H_2O_2 . This research could provide implications in heterogeneous
18 photocatalyst utilization, and shed light on capable combinations between
19 photocatalyst and oxidants in future wastewater treatment under solar light irradiation.

20 **Acknowledgement**

21 Financial support from the National Natural Science Foundation of China (No.
22 21875153 and 21906111), the China Postdoctoral Science Foundation

1 (2019M661933), Natural Science Research of Jiangsu Higher Education Institutions
2 (19KJB610006), and the Young Thousand Talented Program are greatly appreciated.
3 The authors gratefully acknowledge financial support from China Scholarship
4 Council for Xiaoning Wang to study at the University Clermont Auvergne, France.
5 Authors acknowledge financial support from the Region Council of Auvergne, from
6 the “Fédération des Recherches en Environnement” through the CPER
7 “Environment” founded by the Region Auvergne, the French government, FEDER
8 from the European Community from PRC program CNRS/NSFC n°270437 and from
9 CAP 20-25 I-site project.

10

11 **References**

- 12 Abdelmelek, S.B., Greaves, J., Ishida, K.P., Cooper, W.J., Song, W., 2011. Removal of
13 pharmaceutical and personal care products from reverse osmosis retentate using advanced
14 oxidation processes. *Environ. Sci. Technol.* 45, 3665-3671.
- 15 Andreozzi, R., Caprio, V., Insola, A., Marotta, R., 1999. Advanced oxidation processes (AOP) for
16 water purification and recovery. *Catal. Today* 53, 51-59.
- 17 Andreozzi, R., Caprio, V., Marotta, R., Vogna, D., 2003. Paracetamol oxidation from aqueous
18 solutions by means of ozonation and H₂O₂/UV system. *Water Res.* 37, 993-1004.
- 19 Brigante, M., Charbouillot, T., Vione, D., Mailhot, G., 2010. Photochemistry of
20 1-Nitronaphthalene: a potential source of singlet oxygen and radical species in atmospheric waters.
21 *J. Phys. Chem. A* 114, 2830-2836.
- 22 Buxton, G.V.; Greenstock, C.L.; Helman, W.P.; Ross, A.B., 1988. Critical review of rate constants
23 for reactions of hydrated electrons, hydrogen atoms and hydroxyl radicals ($\cdot\text{OH}/\cdot\text{O}$) in aqueous
24 solution. *J. Phys. Chem. Ref. Data* 17, 513-886
- 25 de Luna, M.D.G., Briones, R.M., Su, C.-C., Lu, M.-C., 2013. Kinetics of acetaminophen
26 degradation by Fenton oxidation in a fluidized-bed reactor. *Chemosphere* 90, 1444-1448.
- 27 Deng, J., Shao, Y., Gao, N., Xia, S., Tan, C., Zhou, S., Hu, X., 2013. Degradation of the
28 antiepileptic drug carbamazepine upon different UV-based advanced oxidation processes in water.
29 *Chem. Eng. J.* 222, 150-158.
- 30 Elliot, A.J., 1992. A pulse radiolysis study of the reaction of OH with I₂ and the decay of I₂⁻. *Can. J.*
31 *Chem.-Rev. Can. Chim.* 70, 1658-1661.
- 32 Esplugas, S., Gimenez, J., Contreras, S., Pascual, E., Rodríguez, M., 2002. Comparison of
33 different advanced oxidation processes for phenol degradation. *Water Res.* 36, 1034-1042.

1 Fang, G.-D., Dionysiou, D.D., Zhou, D.-M., Wang, Y., Zhu, X.-D., Fan, J.-X., Cang, L., Wang,
2 Y.-J., 2013a. Transformation of polychlorinated biphenyls by persulfate at ambient temperature.
3 *Chemosphere* 90, 1573-1580.

4 Fang, G.-D., Dionysiou, D.D., Al-Abed, S.R., Zhou, D.-M., 2013b. Superoxide radical driving the
5 activation of persulfate by magnetite nanoparticles: Implications for the degradation of PCBs.
6 *Appl. Catal. B* 129, 325-332.

7 Gao, X., Zhang, X., Wang, Y., Peng, S., Yue, B., Fan, C., 2015. Photocatalytic degradation of
8 carbamazepine using hierarchical BiOCl microspheres: Some key operating parameters,
9 degradation intermediates and reaction pathway. *Chem. Eng. J.* 273, 156-165.

10 Grebel, J.E., Pignatello, J.J., Mitch, W.A., 2010. Effect of halide ions and carbonates on organic
11 contaminant degradation by hydroxyl radical-based advanced oxidation processes in saline waters.
12 *Environ. Sci. Technol.* 44, 6822-6828.

13 Huang, W., Brigante, M., Wu, F., Mousty, C., Hanna, K., Mailhot, G., 2013. Assessment of the Fe
14 (III)-EDDS complex in Fenton-like processes: from the radical formation to the degradation of
15 bisphenol A. *Environ. Sci. Technol.* 47, 1952-1959.

16 Huang W., Bianco A., Brigante M., Mailhot G., 2018. UVA-UVB activation of hydrogen peroxide
17 and persulfate for advanced oxidation processes: Efficiency, mechanism and effect of various
18 water constituents. *J. Hazard. Mater.* 347, 279-287.

19 Huber, M.M., Canonica, S., Park, G.-Y., Von Gunten, U., 2003. Oxidation of pharmaceuticals
20 during ozonation and advanced oxidation processes. *Environ. Sci. Technol.* 37, 1016-1024.

21 Ji, Y., Zhou, L., Zhang, Y., Ferronato, C., Brigante, M., Mailhot, G., Yang, X., Chovelon, J.M.,
22 2013. Photochemical degradation of sunscreen agent 2-phenylbenzimidazole-5-sulfonic acid in
23 different water matrices. *Water Res.* 47, 5865-5875.

24 Jiang, J., Zhao, K., Xiao, X., Zhang, L., 2012. Synthesis and facet-dependent photoreactivity of
25 BiOCl single-crystalline nanosheets. *J. Am. Chem. Soc.* 134, 4473-4476.

26 Kozmér, Z., Arany, E., Alapi, T., Takács, E., Wojnárovits, L., Dombi, A., 2014. Determination of
27 the rate constant of hydroperoxyl radical reaction with phenol. *Radiat. Phys. Chem.* 102, 135-138.

28 Li, X., Chen, C., Zhao, J., 2001. Mechanism of Photodecomposition of H₂O₂ on TiO₂ Surfaces
29 under Visible Light Irradiation. *Langmuir* 17, 4118-4122.

30 Li, Y., Pan, Y., Lian, L., Yan, S., Song, W., Yang, X., 2017. Photosensitized degradation of
31 acetaminophen in natural organic matter solutions: The role of triplet states and oxygen. *Water Res.*
32 109, 266-273.

33 Li, Y., Song, W., Fu, W., Tsang, D.C.W., Yang, X., 2015. The roles of halides in the acetaminophen
34 degradation by UV/H₂O₂ treatment: Kinetics, mechanisms, and products analysis. *Chem. Eng. J.*
35 271, 214-222.

36 Liang, J., Shan, C., Zhang, X., Tong, M., 2015. Bactericidal mechanism of BiOI-AgI under visible
37 light irradiation. *Chem. Eng. J.* 279, 277-285.

38 Motohashi, N., Saito, Y., 1993. Competitive measurement of rate constants for hydroxyl radical
39 reactions using radiolytic hydroxylation of benzoate. *Chem. Pharm. Bull.* 41, 1842-1845.

40 Neyens, E., Baeyens, J., 2003. A review of classic Fenton's peroxidation as an advanced oxidation
41 technique. *J. Hazard. Mater.* 98, 33-50.

42 Nie, M., Yang, Y., Zhang, Z., Yan, C., Wang, X., Li, H., Dong, W., 2014. Degradation of
43 chloramphenicol by thermally activated persulfate in aqueous solution. *Chem. Eng. J.* 246,
44 373-382.

1 Nie, M., Zhang, W., Yan, C., Xu, W., Wu, L., Ye, Y., Hu, Y., Dong, W., 2019. Enhanced removal of
2 organic contaminants in water by the combination of peroxymonosulfate and carbonate. *Sci. Total.*
3 *Environ.* 647, 734-743.

4 Noorisepehr, M., Ghadirinejad, K., Kakavandi, B., Ramazanpour Esfahani, A., Asadi, A., 2019.
5 Photo-assisted catalytic degradation of acetaminophen using peroxymonosulfate decomposed by
6 magnetic carbon heterojunction catalyst. *Chemosphere* 232, 140-151.

7 Pera-Titus, M., Garcia-Molina, V., Baños, M.A., Giménez, J., Esplugas, S., 2004. Degradation of
8 chlorophenols by means of advanced oxidation processes: a general review. *Appl. Catal. B* 47,
9 219-256.

10 Rosenfeldt, E.J., Linden, K.G., 2004. Degradation of endocrine disrupting chemicals bisphenol A,
11 ethinyl estradiol, and estradiol during UV photolysis and advanced oxidation processes. *Environ.*
12 *Sci. Technol.* 38, 5476-5483.

13 Sarwan, B., Pare, B., Acharya, A.D., Jonnalagadda, S.B., 2012. Mineralization and toxicity
14 reduction of textile dye neutral red in aqueous phase using BiOCl photocatalysis. *J. Photoch.*
15 *Photobio. B* 116, 48-55.

16 Shaban, Y.A., El Sayed, M.A., El Maradny, A.A., Al Farawati, R.K., Al Zobidi, M.I., 2013.
17 Photocatalytic degradation of phenol in natural seawater using visible light active carbon modified
18 (CM)-n-TiO₂ nanoparticles under UV light and natural sunlight illuminations. *Chemosphere* 91,
19 307-313.

20 Tamtam, F., Chiron, S., 2012. New insight into photo-bromination processes in saline surface
21 waters: the case of salicylic acid. *Sci. Total. Environ.* 435-436, 345-350.

22 Tan, C., Gao, N., Zhou, S., Xiao, Y., Zhuang, Z., 2014. Kinetic study of acetaminophen
23 degradation by UV-based advanced oxidation processes. *Chem. Eng. J.* 253, 229-236.

24 Tian, F., Li, G., Zhao, H., Chen, F., Li, M., Liu, Y., Chen, R., 2019. Residual Fe enhances the
25 activity of BiOCl hierarchical nanostructure for hydrogen peroxide activation. *J. Catal.* 370,
26 265-273.

27 Tsujimoto, Y., Hashizume H., Yamazaki M., 1993. Superoxide radical scavenging activity of
28 phenolic compounds. *Int. J. Biochem.* 25, 491-494.

29 Wang, X., Zhang, Z., Xue, Y., Nie, M., Li, H., Dong, W., 2014. Low crystallized BiOCl_{0.75}I_{0.25}
30 synthesized in mixed solvent and its photocatalytic properties under simulated solar irradiation.
31 *Mater. Lett.* 136, 30-33.

32 Wang, X., Bi, W., Zhai, P., Wang, X., Li, H., Mailhot, G., Dong, W., 2016a. Adsorption and
33 photocatalytic degradation of pharmaceuticals by BiOCl_xI_y nanospheres in aqueous solution. *Appl.*
34 *Surf. Sci.* 360, 240-251.

35 Wang, X., Chen, H., Li, H., Mailhot, G., Dong, W., 2016b. Preparation and formation mechanism
36 of BiOCl_{0.75}I_{0.25} nanospheres by precipitation method in alcohol–water mixed solvents. *J. Colloid*
37 *Interf. Sci.* 478, 1-10.

38 Wang, X., Brigante, M., Mailhot, G., Dong, W., 2018. Bismuth catalyst mediated degradation of
39 p-hydroxyphenylacetic acid: Photoactivation, interfacial mechanism, and influence of some
40 critical parameters. *Chem. Eng. J.* 349, 822-828.

41 Wu, Y., Bianco, A., Brigante, M., Dong, W., de Sainte-Claire, P., Hanna, K., Mailhot, G., 2015a.
42 Sulfate Radical Photogeneration Using Fe-EDDS: Influence of Critical Parameters and Naturally
43 Occurring Scavengers. *Environ. Sci. Technol.* 49, 14343-14349.

44 Wu, Y., Prulho, R., Brigante, M., Dong, W., Hanna, K., Mailhot, G., 2017. Activation of persulfate

1 by Fe(III) species: Implications for 4-tert-butylphenol degradation. *J. Hazard. Mater.* 322,
2 380-386.

3 Wu, W., Changzhong, J., Roy, V.A., 2015b. Recent progress in magnetic iron oxide-semiconductor
4 composite nanomaterials as promising photocatalysts. *Nanoscale* 7, 38-58.

5 Xu, L., Yang, L., Bai, X., Du, X., Wang, Y., Jin, P., 2019. Persulfate activation towards organic
6 decomposition and Cr(VI) reduction achieved by a novel CQDs-TiO_{2-x}/rGO nanocomposite.
7 *Chem. Eng. J.* 373, 238-250.

8 Yang L., Yu L.E., Ray M.B., 2008a. Photocatalytic oxidation of paracetamol: dominant reactants,
9 intermediates, and reaction mechanisms. *Environ. Sci. Technol.* 43, 460-465.

10 Yang L., Liya E.Y., Ray M.B., 2008b. Degradation of paracetamol in aqueous solutions by TiO₂
11 photocatalysis. *Water Res.* 42, 3480-3488.

12 Yang, X.-y., Wei, H., Li, K.-b., He, Q., Xie, J.-c., Zhang, J.-t., 2018a. Iodine-enhanced ultrasound
13 degradation of sulfamethazine in water. *Ultrason. Sonochem.* 42, 759-767.

14 Yang, Y., Banerjee, G., Brudvig, G.W., Kim, J.H., Pignatello, J.J., 2018b. Oxidation of Organic
15 Compounds in Water by Unactivated Peroxymonosulfate. *Environ. Sci. Technol.* 52, 5911-5919.

16 Yun, W.-C., Lin, K.-Y.A., Tong, W.-C., Lin, Y.-F., Du, Y., 2019. Enhanced degradation of
17 paracetamol in water using sulfate radical-based advanced oxidation processes catalyzed by
18 3-dimensional Co₃O₄ nanoflower. *Chem. Eng. J.* 373, 1329-1337.

19 Zhang, T., Chu, S., Li, J., Wang, L., Chen, R., Shao, Y., Liu, X., Ye, M., 2017. Efficient
20 Degradation of Aqueous Carbamazepine by Bismuth Oxybromide-Activated Peroxide Oxidation.
21 *Catalysts* 7.

22 Zhang, X., Ai, Z., Jia, F., Zhang, L., 2008. Generalized one-pot synthesis, characterization, and
23 photocatalytic activity of hierarchical BiOX (X= Cl, Br, I) nanoplate microspheres. *J. Phys. Chem.*
24 *C* 112, 747-753.